The Journal of Chemical Physics

Time-dependent atomistic simulations of the CP29 light-harvesting complex

Cite as: J. Chem. Phys. **155**, 055103 (2021); https://doi.org/10.1063/5.0053259
Submitted: 06 April 2021 . Accepted: 16 July 2021 . Published Online: 06 August 2021

Sayan Maity, Pooja Sarngadharan, Vangelis Daskalakis, and Ulrich Kleinekathöfer

The Journal of Chemical Physics ARTICLE scitation.org/journal/jcp

Time-dependent atomistic simulations of the CP29 light-harvesting complex

Cite as: J. Chem. Phys. 155, 055103 (2021); doi: 10.1063/5.0053259
Submitted: 6 April 2021 • Accepted: 16 July 2021 •
Published Online: 6 August 2021

Sayan Maity,[1] Pooja Sarngadharan,[1] Vangelis Daskalakis,[2] and Ulrich Kleinekathöfer[1,a)]

AFFILIATIONS

[1] Department of Physics and Earth Sciences, Jacobs University Bremen, Campus Ring 1, 28759 Bremen, Germany
[2] Department of Chemical Engineering, Cyprus University of Technology, 30 Archbishop Kyprianou Str. 3603, Limassol, Cyprus

[a)] **Author to whom correspondence should be addressed:** u.kleinekathoefer@jacobs-university.de

ABSTRACT

Light harvesting as the first step in photosynthesis is of prime importance for life on earth. For a theoretical description of photochemical processes during light harvesting, spectral densities are key quantities. They serve as input functions for modeling the excitation energy transfer dynamics and spectroscopic properties. Herein, a recently developed procedure is applied to determine the spectral densities of the pigments in the minor antenna complex CP29 of photosystem II, which has recently gained attention because of its active role in non-photochemical quenching processes in higher plants. To this end, the density functional-based tight binding (DFTB) method has been employed to enable simulation of the ground state dynamics in a quantum-mechanics/molecular mechanics (QM/MM) scheme for each chlorophyll pigment. Subsequently, the time-dependent extension of the long-range corrected DFTB approach has been used to obtain the excitation energy fluctuations along the ground-state trajectories also in a QM/MM setting. From these results, the spectral densities have been determined and compared for different force fields and to spectral densities from other light-harvesting complexes. In addition, time-dependent and time-independent excitonic Hamiltonians of the system have been constructed and applied to the determination of absorption spectra as well as exciton dynamics.

INTRODUCTION

Chlorophylls (Chl), bacterio-chlorophylls (BChl), and carotenoids (Car) are the key pigment molecules involved in excitation energy transfer (EET) processes in light-harvesting (LH) complexes of plants and bacteria. Actively involved are mainly the low-lying excited states of these pigment molecules. The aim of these processes is to transport the energy absorbed from the sunlight to reaction centers where charge separation takes place as one of the steps of photosynthesis.[1] In the last two decades, the interest in some LH complexes of bacteria and marine algae has been spurred due to the claim of experimentally observed long-lived quantum coherences in EET processes at low as well as at ambient temperatures.[2–6] Recently, however, it became clear that these long-lived oscillations likely originate from impulsively excited vibrations and are too short-lived to have any functional significance in photosynthetic energy transfer.[6–8]

Independent of these developments, the attention toward plant LH systems has significantly increased in recent years. In particular, the topic of photoprotection became a field of growing interest. Under the stress of excess solar energy, LH complexes of plants activate a mechanism termed non-photochemical quenching (NPQ), which can be invoked to avoid photo-inhibition.[9–11] Excess sunlight leads to an enlarged pH gradient across the thylakoid membrane containing the LH complexes of the photosystem II (PSII). An increased pH gradient triggers the switching between the photochemical light harvesting and a non-photochemical quenching mode.[12–15] Moreover, not only the pH gradient but also the presence of a protein termed photosystem II subunit S (PsbS) induces conformational changes in the antenna complexes and thus take part in activating the quenching mechanism.[16–19] The detailed changes in the conformations are, however, still not well understood at the molecular level. The excess sunlight absorbed by the Chl molecules gets released as heat via carotenoid pigments in a mechanism that is a topic of active research.[9,12,20] Based on experimental findings, it has been claimed that the major antenna LHCII and the minor antennas, especially the CP29 complex, play a crucial role in protecting the photosynthetic apparatus of PSII from excess excitation energy.[11–13,19,21,22] At the same time, CP29

acts as a bridge between LHCII and the reaction center core of PSII.

In order to study the dynamics of the LH systems of plants, various models were built based on crystal structures of the LHCII[23–27] and CP29 complexes.[28–33] Furthermore, additional models were created taking into account the lumenal pH gradient and the presence of PsbS proteins trying to realistically mimic the NPQ process.[34–38] In these models, either the population transfer of excitons[39,40] or the associated rates were determined.[33,34] The major input parameters that are required in such calculations are the excitation energies of the individual pigments, also known as site energies, the excitonic couplings between the pigments and the so-called spectral densities. In the present study, the latter quantity is in the focus, while also some of the parameters are being determined.

The spectral density is the key ingredient for performing exciton dynamics of LH complexes within the framework of open quantum systems.[41] It accounts for effects of the pigment environment but also internal modes on the energy gap between ground and first excited states. The accurate determination of spectral densities is, however, a challenging task especially for LH systems due to the complexity of these entities and the numerical effort involved. One approach to determine spectral densities, which has been employed in several previous investigations,[42–46] is to determine the excitation energy gap along a classical MD trajectory using ZINDO/S-CIS (Zerner's Intermediate Neglect of Differential Orbital method with spectroscopic parameters together with the configuration interaction using single excitation) or TDDFT (time-dependent density functional theory) calculations. This approach, however, has problems especially in the high frequency region of the respective spectral densities.[47,48] The shortcoming is due the inability of classical force fields to accurately describe the vibrational modes of the pigments as well as to provide a proper sampling of the geometrical phase space. Inaccuracies in the ground state conformations and dynamics are subsequently passed on to the determination of the energy gap fluctuations. The inconsistency in geometry between the ground and excited state is commonly known as the "geometry mismatch" problem.[49] Some recent methods to determine the intramolecular vibrational modes accurately are based on normal mode analyses[47,50] or ground state dynamics on pre-calculated quantum mechanical potential energy surfaces[51,52] and have been employed in calculations of spectral densities. In spite of providing impressive agreements compared to experimental results, these aforementioned schemes are computationally still demanding.[51,53] A sophisticated quantum-mechanics/molecular mechanics (QM/MM) MD with an accurate description of the vibrational properties of the pigments would be an alternative way; however, semi-empirical schemes have a limited accuracy,[54] while DFT-based calculations are numerically expensive for pigments in LH systems.[55] To this end, we recently proposed a scheme using QM/MM MD dynamics employing the numerically efficient density functional-based tight binding (DFTB) approach[56] and have shown to be able to obtain a good agreement between the spectral densities obtained in such a manner and their experimental counterparts.[48,57]

In this study, we have applied a recently developed multiscale protocol to determine the spectral densities of the individual pigments within the minor antenna complex CP29 of the PSII system. The CP29 complex contains a total of 13 chlorophyll molecules

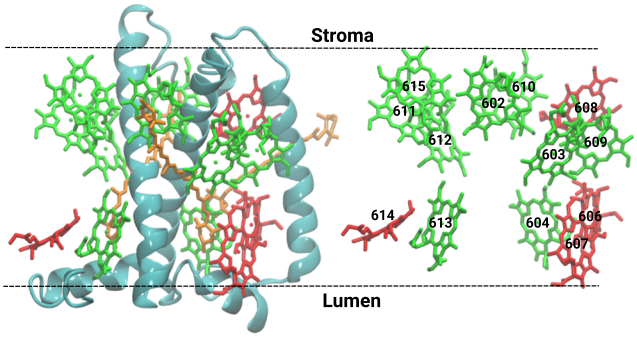

FIG. 1. Protein part of the CP29 minor antenna complex of spinach represented in an ice-blue cartoon representation. The Chl-a and Chl-b molecules are depicted in green and red, while the carotenoids Lut, Vio, and Neo are shown in orange. In addition, the arrangement of the chlorophylls is displayed in the right panel together with the respective residue numbering according to the crystal structure[28] (pdb code: 3PL9).

including nine Chl-a and four Chl-b. In addition, three different types of carotenoids, i.e., lutein (Lut), violaxanthin (Vio), and neoxanthin (Neo), are present in this antenna complex (see Fig. 1). The Chl-b chromophores in the periphery of the protein matrix act as accessory pigments transferring the absorbed light energy toward the pool of Chl-a molecules quite rapidly since the excited states of the latter pigments are slightly lower in energy. From the Chl-a molecules, the energy obtained during light harvesting is moved on to the PSII reaction center. While the carotenoids are speculated to participate in the quenching process, here the aim is to accurately determine the spectral densities for the key pigments, i.e., the chlorophyll molecules in the CP29 complex. To this end, the AMBER force field has been employed in connection with the DFTB approach in a QM/MM framework. The details of the computational scheme can be found in the section titled Computational method. The spectral density profiles obtained in the present calculations show a very good agreement with the experimental counterparts in line with our previous work for other LH systems.[48,57] Furthermore, the impact of the choice of the classical force field in the QM/MM setting has been investigated by redoing the calculations using the OPLS (optimized potentials for liquid simulations) force field in connection with the DFTB method. Only very small differences can be seen in the spectral density profiles when using the two different force fields within the QM/MM framework. This finding indicates that both force fields are suitable for the modeling LH complexes. The present study also incorporates a brief comparison of the spectral densities of the BChl and Chl pigments in different LH systems. Before concluding, we report on time-averaged and time-dependent exciton Hamiltonians and on ensemble-averaged wave packet dynamics within the Ehrenfest formalism for the exciton transfer in the CP29 complex.

COMPUTATIONAL METHOD

The x-ray crystal structure of the CP29 antenna complex from spinach (pdb code: 3PL9)[28] has been used as the starting point for

the atomistic modeling. The first 87 residues were not resolved in the x-ray structure and neglected in the present study since their influence on the spectral densities is assumed to be small. Furthermore, the glyceraldehyde 3-phosphate (G3P) molecule that was tentatively found in between Chl-a 611 and 615 was not taken into account during the system preparation. The AMBER03 force field[58] has been employed for the protein using the GROMACS-5.1.4 suite of programs[59] for the simulations. Moreover, the force field parameters for Chl-a/b[60,61] and carotenoids[62] have been taken from previous studies. First, a POPC lipid membrane was prepared using the CHARMM-GUI server,[63] and then the topology for the membrane was generated using the LEaP program of AmberTools-20 together with the Lipid-17 force field of AMBER. Thereafter, the topology and coordinates were transformed to the GROMACS format with the help of the ACEPYPE interface.[64] The simulation box size was chosen to be 115 × 115 × 90 Å^3, and the system was solvated with TIP3P water molecules. Furthermore, four potassium ions were added to neutralize the whole system. After preparing the system, an energy minimization was performed using the steepest-descent algorithm to remove close contacts. Subsequently, a 2 ns NVT equilibration was carried out at 300 K with a 1 fs integration time step, keeping position restraints on protein, lipid, and cofactor atoms. Subsequently, a 20 ns NPT run was performed using the same time step and position restraints. After that, another 10 ns NPT simulation was run keeping the restraints on protein, pigments, and the phosphorous atoms of the lipid molecules. An additional 10 ns NPT run was carried out using a 1 fs time step, in which the first 5 ns was performed with restraints on protein and pigments, whereas for the last 5 ns the restraints were only on the protein and Chl molecules. Subsequently, in the next 5 ns NPT equilibration, the position restraint was kept only on the protein and the Mg atoms of Chl pigments. Subsequently, yet another 5 ns NPT run was performed using a 2 fs time step, in which the position restraints were kept on the protein for the first 2 ns, then for 1 ns on the side chains atoms, and for 1 ns on the Cα atoms of the protein. Finally, a 50 ns long NPT unbiased simulation was carried out without any position restraints and the coordinates were stored using a 25 ns stride, which were subsequently employed as starting structures for the QM/MM MD simulations in the next step. The LINCS algorithm was applied, and the constraints were kept on the H-bonds throughout the equilibration process. The equilibrated structure was further equilibrated for another 200 ns where the coordinates were stored at 20 ps. This produces 10 000 frames which were utilized for the excitonic coupling calculations using the TrESP (transition charges from electrostatic potentials) approach[65,66] in order to construct the system Hamiltonian. A shift in the position of pigment Chl-a 615 was observed after the classical simulations (see Fig. 2). Structurally, this pigment is solvent exposed in the case of an isolated CP29 crystal structure and thus can more easily move than a pigment embedded in the middle of the protein. A movement by 3.97 Å was found after the 100 ns equilibration, whereas after the 200 ns production run the movement was by 7.12 Å. This finding is consistent with the latest cryo-EM structure of the $C_2S_2M_2$ supercomplex,[67] in which a different Chl-a 601 was found close to the position where Chl-a 615 was found in the x-ray structure used in the present study.[28] Thus, we assume that the contribution of Chl-a 615 will be similar to that of the Chl-a 601 found in the latter case.

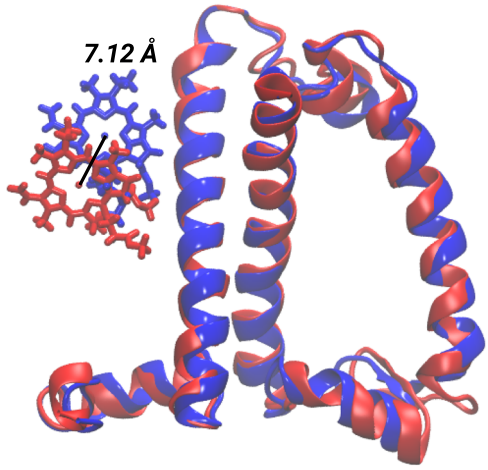

FIG. 2. Structural shift of the pigment Chl-a 615 after the 300 ns classical unbiased simulation (red) compared to the crystal structure used as a starting structure (blue).

Two sets of QM/MM MD simulations, based on starting geometries extracted at 25 and 50 ns from the unbiased classical simulations, were performed to minimize the sampling problems of spectral densities found earlier for the present kind of simulations.[48] A 80 ps NPT QM/MM dynamics was performed with a 0.5 fs integration time step without any bond constraints for the Chl-a and Chl-b molecules. The phytyl tail was truncated at the so-called "C1–C2" bond and capped by a hydrogen link atom. This truncation is sensible since the tails play no role in the π-conjugated rings, but their partial charges potentially influence the Q_y excitation energies of the Chl molecules and thus need to be included in the MM part. Such a treatment significantly reduces the computational costs compared to a full QM treatment of the Chl molecules.[68] DFTB3 theory[69] with the frequency corrected 3OB parameter set (3OB-f)[70] was employed coupled to an AMBER force field as implemented in the GROMACS-DFTB + interface for the ground state dynamics.[71,72] The 3OB-f parameter set was specially designed in connection with the so-called 3OB parameters to describe the vibrational frequencies of C=C, C=N, and C=O bond stretching modes more accurately. These modes are very relevant for molecules including porphyrin rings such as Chl pigments. The last 60 ps of each trajectory was stored with a stride of 1 fs. This procedure results in 2 × 60 000 frames for each Chl molecule using the two different starting structures of the QM/MM MD trajectories. In addition, we extended the first set of simulations up to 1.1 ns with a 1 fs integration time step and stored the geometries for the last 1 ns dynamics with a stride of 100 fs. Thus, another 10 000 frames were generated, which were mainly utilized to calculate the average site energies of the CP29 complex. Furthermore, the CP29 complex, as modeled using the OPLS force field in a previous study,[37] was used as a starting structure for QM/MM MD simulations. Again, two different starting structures were considered as the initial geometries for the QM/MM dynamics. This time the starting structure was 10 ns apart in the unbiased trajectories. Again, we have stored 2 × 60 000 frames for each Chl pigment in order to perform the spectral density calculations.

The snapshots collected from the DFTB-QM/MM MD trajectories were utilized to calculate the Q_y excitation energies employing the time-dependent extension of the long-range corrected DFTB (TD-LC-DFTB) in a QM/MM fashion. The LC-DFTB method is the DFTB analog of the long-range corrected DFT (LC-DFT) approach with functionals such as CAM-B3LYP and ωB97X, which has lately been developed to overcome problems related to charge transfer and overpolarization in conjugated systems.[73] In recent studies, we have shown that TD-LC-DFTB is a close to ideal alternative to DFT with long-range corrected functionals in order to compute excitation energies and excitonic couplings in a numerically efficient way.[68] To this end, we have employed the DFTB + package in which the TD-LC-DFTB scheme is implemented based on the OB2 parameter set.[72,73] Moreover, during the excitation energy calculations the QM region is shifted toward the center of the simulation box to avoid boundary problems during the non-periodic QM/MM calculations. After capturing the excitation energies along the QM/MM trajectories, these were used to determine the autocorrelation functions from which the spectral densities were calculated by performing Fourier transformations as described below.

The excitonic couplings have been determined based on the 200 ns classical MD simulation. 10 000 snapshots were collected and utilized for the TrESP excitonic coupling calculations as described below. For this purpose, the transition charges for the Chl-a and Chl-b molecules were determined with the help of the Multiwfn[74] and the ORCA[75] packages. Transition charges of these molecules exist,[30] but we repeat them here with a long-range corrected functional and a larger basis set. First, a geometry optimization was performed at the B3LYP level of theory together with a def2-TZVP basis set as implemented in the ORCA program. Furthermore, the resolution of identity RIJCOSX was employed together with the auxiliary basis set def2/J in order to speed up the calculations. In a subsequent step, the optimized geometries were utilized to perform excited state TD-DFT calculation employing the Tamm–Dancoff approximation at the CAM-B3LYP level of theory as implemented in ORCA. The same basis set and the resolution identity were applied again for these calculations. Finally, the transition densities obtained from the TD-DFT calculations were used in the Multiwfn package for the electrostatic fitting. During the fitting procedure, the charges on the hydrogen atoms were set to zero and the transition densities were distributed among the heavier atoms of the Chl-a and Chl-b molecules. The obtained TrESP charges are listed in the supplementary material (see Table S1) and were used in the TrESP calculations for the excitonic couplings. Moreover, we have employed scaling factors of 0.81 for the Chl-a charges and 0.83 for the Chl-b charges in order to reproduce the experimental transition dipole moments of 5.7 and 4.6 D, respectively.[76]

THEORETICAL BACKGROUND

To be able to determine the exciton dynamics in LH complexes within a tight-binding model, one needs to construct the excitonic system Hamiltonian based on the site energies E_m of the pigments m and the respective couplings V_{nm},[41]

$$H_S = \sum_m E_m |m\rangle\langle m| + \sum_{n\neq m} V_{mn} |n\rangle\langle m|. \tag{1}$$

If the site energies and coupling are determined based on (quantum) molecular dynamics trajectories, these quantities are time-dependent. Two main options are available how to determine the exciton dynamics. One option is to perform calculations directly based on these time-dependent Hamiltonians, e.g., some kind of ensemble-averaged Ehrenfest approach (without back reaction on the bath)[77] sometimes also termed NISE (numerical integration of the Schrödinger equation).[78] In the present study, we refrain from introducing correction factors trying to fix this problem of missing thermalization in these approaches.[77,78] These problems are not present if one uses proper density matrix approaches. To this end, one averages the elements of the Hamiltonian over time. The site energy fluctuations are then represented by the so-called spectral density. In principle, one can also define spectral densities for the coupling fluctuations, but this is very rarely done since the effect of these fluctuations on the dynamics is negligible.[79] On the experimental side, spectral densities corresponding to those based on the excitation energy fluctuations can be obtained using delta fluorescence line narrowing (ΔFLN) spectroscopy. In the present study, we employ a cosine transformation of the energy autocorrelation functions decorated with a thermal prefactor to determine the spectral density,[42,44,80]

$$J_m(\omega) = \frac{\beta\omega}{\pi} \int_0^\infty dt\ C_m(t) \cos(\omega t), \tag{2}$$

with $\beta = 1/(k_B T)$. The necessary autocorrelation functions for each pigment m can be written as

$$C_m(t_l) = \frac{1}{N-l} \sum_{k=1}^{N-l} \Delta E_m(t_l + t_k) \Delta E_m(t_k). \tag{3}$$

Here, ΔE_m denotes the difference of site energy E_m from its average value $E_m = E_m - \langle E_m \rangle$ and N is the number of snapshots present in the respective part of the trajectory. Moreover, we follow the same procedure as detailed in our previous work[48,57] to obtain the final correlation functions and spectral densities.

For computing excitonic couplings in LH complexes, the TrESP method has been shown to be accurate for medium and large distances. Once the atomic transition charges of the pigment molecules have been determined, the coupling values can be calculated as

$$V_{mn} = \frac{f}{4\pi\epsilon_0} \sum_{I,J}^{m,n} \frac{q_I^T \cdot q_J^T}{|\, r_m^I - r_n^J \,|}, \tag{4}$$

where q_I^T and q_J^T denote the transition charges of atoms I and J and f is a distance-dependent screen factor taking environmental influences on the excitonic coupling into account. For this reason, here we have employed a well-established exponential screening factor derived by Scholes *et al.*,[81]

$$f(R_{mn}) = A\ \exp(-BR_{mn} + f_0). \tag{5}$$

In this expression, A, B, and f_0 have the values 2.68, 0.27, and 0.54, respectively.[81] We note that this kind of empirical screening factor takes only explicit effects (cavity effect and screening of interaction) into account but not of implicit effects (enhancement of transition dipole moments by environment).[81] Thus, the chosen screening function is not perfect and one could also consider other empirical

screening functions such as distance-independent ones. The effect of choosing other reasonable empirical screening functions should, however, be limited.

RESULTS AND DISCUSSION

Site energy calculations

As a starting point of the analysis, the average site energies of the 13 Chl molecules have been determined for the three QM/MM MD trajectories. The structurally very similar Chl-a and Chl-b pigments contain Mg-porphyrin rings, which are mainly responsible for the electronic properties of the respective molecules and especially the excited Q_y state. When the methyl group of a Chl-a porphyrin ring is oxidized to become an aldehyde group, the molecules become Chl-b molecules with a blue shift in the excitation energies (see Fig. S1). Due to the higher Q_y excitation energies of Chl-b molecules, excitation energy from these pigments will, depending on the respective couplings, flow to neighboring Chl-a molecules. The energy is subsequently shared between the Chl-a molecules and transferred further into the direction of lower energies ending up at a reaction center. In the present study, the TD-LC-DFTB approach has been employed as the QM approach to compute the excitation energies for the individual Chl molecules along the QM/MM MD trajectories. As for basically all DFT approaches, the energy gaps are overestimated, which are in line with our previous observations.[48,57,68] In many cases, this does, however, not cause problems since we are mainly interested in the relative site energies. The energy ladder and the corresponding standard deviations due to the thermal fluctuations along the two different 60 ps-long and the one 1 ns long QM/MM MD trajectories are shown in Fig. 3(a). The results for the average site energies of the individual pigments are almost identical for the three different trajectories. Although the 1 ns QM/MM MD trajectory is averaging over a much longer time span than the 60 ps runs, no significant differences are observed. The respective distributions for the site energies that are also known as the densities of states (DOSs) are depicted in Figs. S2 and S3. The shape of these distributions is Gaussian, i.e., symmetric, and not skewed as observed in similar calculations using the semi-empirical ZINDO/S-CIS approach.[43,46] As expected, the average site energies of the Chl-b pigments are higher in energy than the Chl-a molecules, although the spectral densities for these two types of molecules are almost identical as shown below. The structural difference between the Chl-a and b molecules has already been mentioned above and, as depicted in Fig. S1, is the only reason behind the blue shifted site energies of Chl-b molecules. Furthermore, the excitation energy fluctuations of the Chl-a molecules are in the same range as those found for the same pigment type in the LHCII complex.[57] Moreover, we have compared the calculated site energies with literature results, as shown in Fig. 3(b). In the case of the results by Jurinovich *et al.*,[31] TD-DFT calculations were carried out along the classical MD trajectory based on the CAM-B3LYP/6-31G(d) level of theory within a polarizable QM/MM description. Since CAM-B3LYP is a long-range corrected DFT functional, the site energies obtained employing this approach are quite similar to our TD-LC-DFTB calculations. In the case of the calculations by Müh *et al.*,[30] the results are accurately matching the findings by Jassas *et al.*[82] This agreement is due to the fact that the TrESP approach was applied in both studies to calculate the excitonic couplings and energies. Subsequently, the absorption spectrum was fitted to determine the site energies. However, in the case of the results by Mascoli *et al.*,[83] the site energies differ slightly from the former results due to the utilization of the dipole–dipole approximation to determine the excitonic energies and the corresponding spectrum. As mentioned above, the results based on DFT approaches clearly show an overall overestimation of the excitation energy gaps, which is also reflected in a shift in site energies compared to the experimental outcomes. For this reason, we introduced a common shift for our site energies toward the experimental values and compared with measurements by Jassas *et al.*[82] and Mascoli *et al.*[83] The shifted energies are depicted in Fig. S4.

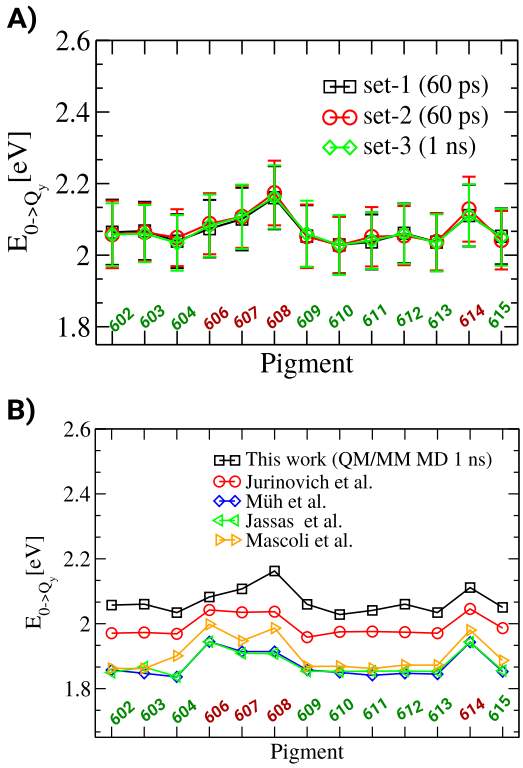

FIG. 3. (a) Average site energies of the Chl molecules in the CP29 complex with the respective error bars indicating the fluctuations along the three different QM/MM MD trajectories. The residues 602, 603, 604, 609, 610, 611, 612, 613, and 615 refer to Chl-a molecules (green), while the residues 606, 607, 608, and 614 refer to Chl-b molecules (red). (b) Comparison with other computed site energies for the CP29 complex by Jurinovich *et al.*,[31] Müh *et al.*,[30] Jassas *et al.*,[82] and Mascoli *et al.*[83]

Autocorrelation functions and spectral densities

The primary step of calculating spectral densities from site energy trajectories is to compute the autocorrelation functions of the site energy fluctuations. Here, we have determined the correlation functions for each Chl-a and Chl-b molecule separately. The autocorrelation functions averaged over the two 60 ps-long

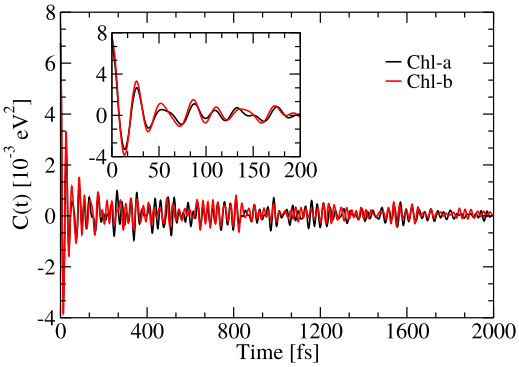

FIG. 4. Average Chl-a and Chl-b autocorrelation functions calculated along the two sets of QM/MM MD trajectories and averaged over the pigments of the same time. The inset highlights the first 200 fs.

QM/MM MD trajectories and the nine Chl-a and the four Chl-b molecules, respectively, are depicted in Fig. 4. From Fig. 4, it is clear that the Chl-a and Chl-b molecules have very similar correlation functions. This was, however, to be expected because of their very similar structures and fluctuations of site energies. The resulting correlation functions show that the shortest oscillation period is around 22–32 fs, which can be attributed to intramolecular collective modes including C=C, C=O, and C=N vibrational stretching in the porphyrin rings. This observation is in line with our previous work on different LH systems based on DFTB-QM/MM MD simulations.[48,57] The associated spectral densities are shown in Fig. 5 for the Chl-a and Chl-b molecules and, as to be expected, also show very similar line shapes. The spectral densities of the individual Chl molecules are shown in Figs. S5 and S6.

Comparison to experimental spectral densities

In experiment, ΔFLN spectroscopy is used to determine the exciton–phonon and exciton–vibrational coupling of pigment molecules. From the fluorescence profiles, the corresponding frequencies ω are extracted together with the respective Huang-Rhys

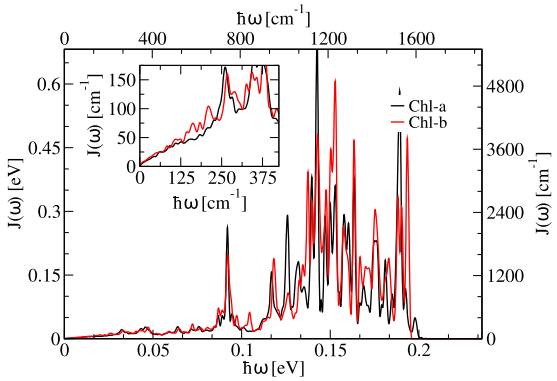

FIG. 5. Spectral densities based on the autocorrelation functions shown in Fig. 4.

(HR) factors. In a subsequent step, these HR factors and the frequencies ω are used to construct the spectral densities. Often these spectral densities are given in the form

$$J^{\mathrm{exp}}(\omega) = J_0^{\mathrm{exp}}(\omega) + J_{vib}^{\mathrm{exp}}(\omega), \tag{6}$$

where $J_0^{\mathrm{exp}}(\omega)$ represents the continuous low frequency component of the spectral density representing the exciton–phonon coupling, i.e., the coupling to the protein and solvent environment. This part is estimated as one over-damped Brownian oscillator. The second part, $J_{vib}^{\mathrm{exp}}(\omega)$, describes the high frequency component consisting of more or less separate parts describing intramolecular vibrations of the pigment molecules. Experimentally, in total 48 vibrational frequencies were extracted for the Chl molecules in the entire PSII system[84] or separately for the LHCII complex,[85] which are generally described by under-damped Brownian oscillators. The first part of the spectral density can be modeled by a log-normal expression,[86]

$$J_0^{\mathrm{exp}}(\omega) = \frac{\hbar\omega S}{\sigma\sqrt{2\pi}} \exp^{-[\ln(\omega/\omega_c)]^2/2\sigma^2}, \tag{7}$$

where the HR factor S, the cut-off frequency ω_c, and the standard deviation σ are given in Fig. 3 of Ref. 86. The second part of the spectral density is specified by a sum of Lorentzian functions given by

$$J_{vib}^{\mathrm{exp}}(\omega) = \frac{2\hbar}{\pi} \sum_k s_k \omega_k^3 \frac{\gamma_k \omega}{(\omega_k^2 - \omega^2)^2 + \gamma_k^2 \omega^2}, \tag{8}$$

where the HR factors s_k and their corresponding frequencies ω_k have been extracted from Table S4 in Ref. 83 for the CP29 complex. Moreover, the broadening factor γ_k has been chosen to be $\hbar\gamma_k = 7\ \mathrm{cm}^{-1}$ (for all k) to obtain intensities of the experimental spectral density peaks similar to those calculated here. This broadening factor γ_k can be chosen freely within certain limits to control the width and intensity of the respective peaks. Moreover, the HR factors utilized for the CP29 complex are the same as for the LHCII complex[85] but scaled by a factor in order to reproduce the fluorescence spectrum.[83] The present procedure of computing spectral densities does not include any broadening factors, while the widths of these peaks are determined through the Fourier transformation of the respective autocorrelation functions.

The comparison of the theoretically calculated average spectral density of the CP29 complex with the experimentally determined one is depicted in Fig. 6(a). Since the average over all pigments washes out some peaks, here we have also compared the experimental results of the entire CP29 complex with the computed one for the individual pigment Chl-a 604 [shown in Fig. 6(b)], which has the lowest site energy in our calculations. In both plots, the simulated spectral density for the CP29 complex shows a remarkable agreement with the experimental results. The major peaks and their amplitudes are matching well, as shown in Fig. 6. This finding agrees well with our previous studies for the Fenna-Matthews-Olson (FMO)[48] and the LHCII complexes.[57] In the low frequency region, however, the amplitude is moderately overestimated. The reason is not entirely clear but may be due to inaccuracies in the classical point charges in the QM/MM simulations and the finite length of the correlation functions since low frequencies correspond

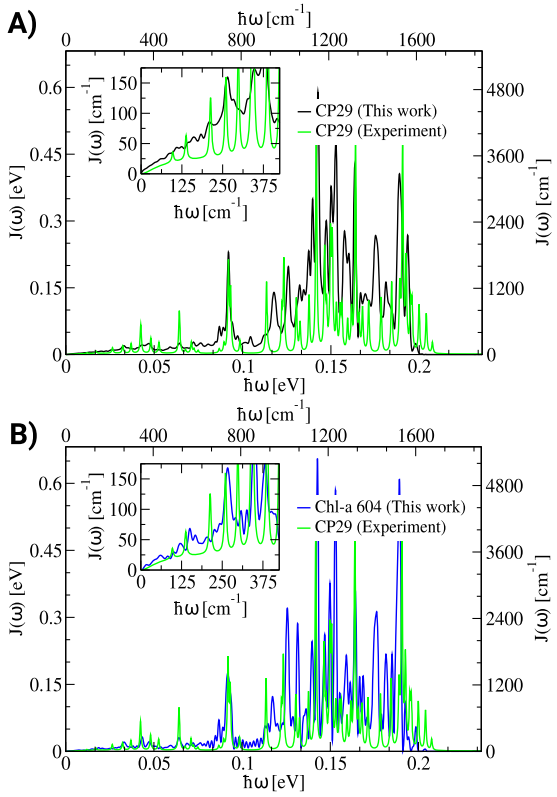

FIG. 6. (a) Average theoretically determined spectral density of the CP29 complex in comparison to the experimental spectral densities of the CP29.[83] The inset enhances the low frequency region. (b) Same as panel (a) but for the single pigment Chl-a 604.

to modes with long periods. Further research in this direction is ongoing.

Impact of the classical force fields on spectral density in the QM/MM MD simulation

The major peaks in the spectral densities lie in the range from 1030 to 1550 cm^{-1} caused by the fastest oscillations in the correlation functions. Here, we would like to point out that in the case of spectral densities based on pure classical force fields, the major peaks were located in the region from 1450 to 1800 cm^{-1} as found in previous work on bacterial LH complexes.[43,44,46,48] Furthermore, the spectral densities for Chl molecules based on the semi-empirical PM6 method in a QM/MM MD dynamics showed a shift in the dominant frequencies by about 100–130 cm^{-1} compared to the experimental results.[54] The inaccurate positions of the high-amplitude peaks in the spectral densities arise due to poor descriptions of the vibrational features using classical force fields or low-level semi-empirical theories. Using DFTB ground state dynamics together with the 3OB-f parameter set, however, leads to a proper description of the most important vibrational frequencies. The choice of the DFTB method rather than DFT approaches becomes necessary due to the high numerical cost of the latter for larger molecules especially when

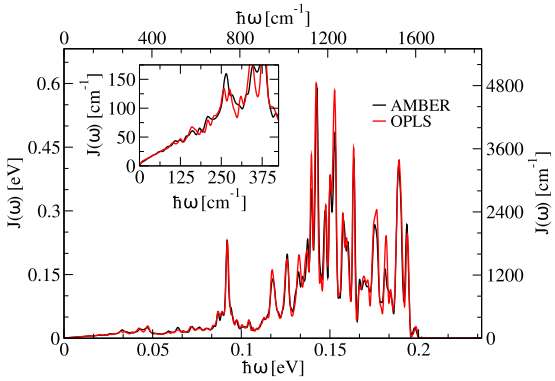

FIG. 7. Average spectral density of the CP29 complex based on the DFTB approach in combination with either the AMBER or the OPLS force field. The inset highlights the low frequency region.

calculating along trajectories. The low frequency part in the spectral densities is due to electrostatic interactions with the environment, i.e., protein as well as water and ions. However, different force field sets follow (partially) unlike parameterization schemes for the partial charges. Since the partial charges are key ingredients in electrostatic QM/MM schemes as employed in the present study, we have analyzed the effect of different force field sets. For the ground state dynamics based only on classical MD simulations, a comparison between CHARMM and AMBER-compatible force fields has been performed earlier.[87] Although quite some differences between the spectral densities were seen in that case, one has to keep in mind that the parameterization of the pigment molecules was of large importance. For this reason, in the present case, we have utilized a setup of the CP29 complex pre-equilibrated using the OPLS force field[37] and determined the spectral densities in the same way as for the AMBER force field in a QM/MM fashion. As can be seen in Fig. 7, the average spectral density based on the OPLS force field shows an almost identical profile to that one based on the AMBER force field in the QM/MM simulations. The positions of the peaks are at the same for both variants since these basically rely on the QM part, i.e., the DFTB approach only, which was the same in both variants. More surprisingly, the contributions in the low frequency part of the spectral density are almost identical, although the environment is described by different force fields, i.e., different sets of partial charges. This finding is probably due to the fact that the partial charges in both force fields are determined by fitting of the electrostatic potentials.[88] The observed similarity between the QM/MM simulations in combination with different force fields suggests that both force fields are equally well suited for the present kind of calculations on LH systems.

Comparison of spectral density for other LH complexes

Furthermore, in order to analyze the accuracy and robustness of our method for LH systems, in Fig. 8, we have compared the average spectral density of the CP29 complex with those of the FMO[48] and LHCII[57] complexes obtained using the same QM/MM procedure. In the case of the LHCII complex, the Chl-a pool was

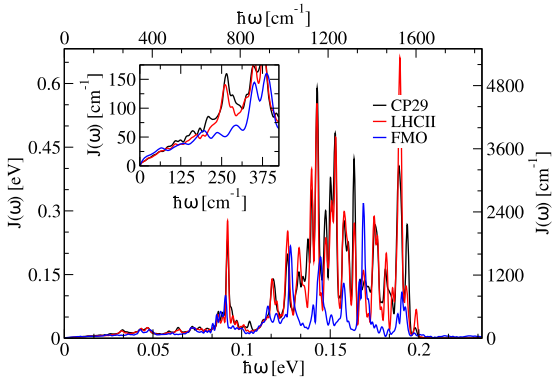

FIG. 8. Average spectral density of the CP29 complex compared to those from the FMO[48] and the LHCII[57] system.

considered for the whole trimeric complex,[57] whereas for FMO, all BChl-a pigments have been taken into account from one monomeric unit of the trimer.[48] As can be seen, the CP29 and LHCII complexes have almost identical average spectral density profiles. This is, however, not too surprising since in both complexes Ch-a and Chl-b are considered, which show almost identical spectral densities as described earlier. In the case of the bacterial FMO complex, however, the amplitudes of the major peaks are lower compared to those of the plant complexes.[48] This finding is consistent with the fact that the range of site energy fluctuations is higher for the Chl molecules in the respective complexes than those of the BChl pigments in the FMO protein. Likely, one of the facts behind this larger site energy fluctuations in plant LH complexes is the larger values of the Q_y excitation energies in Chl molecules; however, further investigation is required to understand this observation in more detail. Moreover, the number of major peaks in the FMO complex is less than for the two plant ones, which seems to be surprising since the porphyrin ring of the BChl molecules is more flexible having one C=C double bond less than the Chl molecules (see Fig. S1). This computational observation is also underlined by experimental measurements since in the case of the FMO complex 62 vibrational peaks were resolved,[89] whereas for the plant systems, 48 peaks were found.[84,85] A comparison between the experimental spectral densities of the FMO and CP29 complexes is shown in Fig. S7. The higher number of vibrational peaks in the experiments suggests that in our calculations, some peaks have probably been washed out during the averaging procedure over all pigments or some peaks might have merged to form a single peak with larger width.

Excitonic coupling and wave packet dynamics

DFTB-QM/MM MD simulations are still computationally expensive when one wants to treat several pigments at a time. Therefore, we have constructed the time-averaged Hamiltonian based on the coupling values calculated from the 200 ns classical MD simulation and the site energies based on the 1 ns QM/MM MD trajectory (see Table I). As described in section titled Computational method, the excitonic couplings between all Chl pigments of the CP29 complex were calculated using the TrESP approach. A total of 10 000 frames from the 200 ns long classical MD trajectory were employed to calculate the coupling values. The distribution of larger coupling values is represented in Fig. 9. Most of the larger coupling values originate from the Chl-a pairs as a consequence of their spatial proximity. In the case of the Chl-b chromophores, pigments 606 and 608 are participating in stronger couplings with Chl-b 606 showing the highest coupling value to neighboring pigments. Once the excitonic couplings have been determined, the system Hamiltonian can be established based on Eq. (1). This time-independent Hamiltonian together with the spectral densities obtained in the present study can serve as a starting point for future calculations using density matrix approaches.

As accurate density matrix calculations are numerically not feasible at present for larger systems with spectral densities as the ones derived here, we have performed ensemble-averaged wave packet dynamics within the Ehrenfest approach (without back reaction of the thermal bath). We note in passing that work is in progress

TABLE I. Time-averaged system Hamiltonian of the CP29 complex based on the exciton coupling values along the 200 ns classical MD trajectory and the site energies from the 1 ns QM/MM MD simulation. The site energies and couplings (in cm^{-1}) with absolute values above 30 cm^{-1} are shown in bold.

	a602	a603	a604	b606	b607	b608	a609	a610	a611	a612	a613	b614	a615
a602	**16 594**	**29.39**	4.13	3.33	1.68	−3.85	−23.10	−5.62	−1.23	7.15	−1.94	0.58	**54.74**
a603	**29.39**	**16 617**	−1.03	−2.97	9.64	2.96	**84.79**	6.35	−0.65	−2.02	0.65	−2.92	−3.57
a604	4.13	−1.03	**16 408**	**72.97**	2.37	−2.05	−0.66	−1.54	−1.93	0.75	0.51	−1.95	−2.13
b606	3.33	−2.97	**72.97**	**16 796**	1.77	−1.93	5.14	−1.18	−1.50	1.11	0.73	−0.84	−1.33
b607	1.68	9.64	−2.37	1.77	**16 997**	−2.17	−8.71	1.87	−1.08	0.13	−1.26	−1.75	−0.23
b608	−3.85	2.96	−2.05	−1.93	−2.17	**17 442**	22.17	**50.39**	3.48	−1.51	−1.42	0.63	3.00
a609	−23.10	**84.79**	−0.66	5.14	−8.71	22.17	**16 612**	−0.92	3.06	−0.25	−2.10	1.28	4.51
a610	−5.62	6.35	−1.54	−1.18	1.87	**50.39**	−0.92	**16 360**	−26.80	**41.58**	5.11	−0.12	−2.78
a611	−1.23	−0.65	−1.93	−1.50	−1.08	3.48	3.06	−26.80	**16 462**	**90.94**	−4.02	−1.18	**43.95**
a612	7.15	−2.02	0.75	1.11	0.13	−1.51	−0.25	**41.58**	**90.94**	**16 617**	−5.94	1.50	−3.73
a613	−1.94	0.65	0.51	0.73	−1.26	−1.42	−2.10	5.11	−4.02	−5.94	**16 409**	−7.38	6.33
b614	0.58	−2.92	−1.95	−0.84	−1.75	0.63	1.28	−0.12	−1.18	1.50	−7.38	**17 030**	−10.65
a615	**54.74**	−3.57	−2.13	−1.33	−0.23	3.00	4.51	−2.78	**43.95**	−3.73	6.33	−10.65	**16 537**

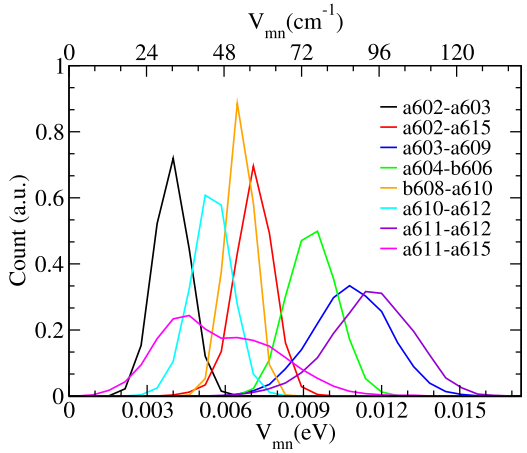

FIG. 9. Distribution of excitonic coupling values for the pigment pairs whose average absolute values are above 30 cm^{-1}.

trying, e.g., by our group, to derive density matrix approaches, which can handle numerically obtained spectral densities.[90] For certain parameter regimes, however, the Ehrenfest (NISE) wave packet approach has been shown to yield the same results as accurate density matrix calculations properly representing the dephasing but not the relaxation.[77] In the wave packet-based scheme, the time-dependent Schrödinger equation needs to be solved for the time-dependent system Hamiltonian,

$$i\hbar\frac{\partial|\Psi_S(t)\rangle}{\partial t} = H_S(t)|\Psi_S(t)\rangle, \tag{9}$$

where $|\Psi_S(t)\rangle$ denotes an excitonic state in the single-exciton manifold. This state can be expanded in terms of time-independent states $|\alpha\rangle$,

$$|\Psi_S(t)\rangle = \sum_\alpha c_\alpha(t)|\alpha\rangle, \tag{10}$$

with time-dependent coefficients $c_\alpha(t)$. Moreover, the excitonic states $|\alpha\rangle$ can be written in terms of site-local states $|m\rangle$ as

$$|\alpha\rangle = \sum_m c_m^\alpha|m\rangle. \tag{11}$$

Combining these equations, the probability density of finding an exciton on an individual pigment site m is given by

$$P_m(t) = |\langle m|\Psi_S(t)\rangle|^2 = |\sum_\alpha c_m^\alpha.c_\alpha(t)|^2. \tag{12}$$

The dynamics of the probability density $P_m(t)$ shows how an exciton can propagate from pigment to pigment and spread at the same time. To obtain meaningful exciton transfer dynamics, the solution of the time-dependent Schrödinger equation needs to be repeated many times from a different starting point along the trajectory to obtain ensemble-averaged results.

In the case of the CP29 complex, we have taken the average coupling values calculated from the 200 ns classical MD simulation together with the site energies obtained from the first set of the 60 ps QM/MM MD trajectories to propagate the wave packet dynamics. This leads to a realistic time-dependent Hamiltonian for the 60 ps trajectory since the coupling fluctuations hardly impact the exciton propagation as shown in earlier studies.[48,79] Furthermore, for the averaging procedure, we have assumed that the temporal site energy fluctuations are basically uncorrelated after 500 fs (see also Fig. 3). Thus, every 500 fs a new starting point in the trajectory is used for the averaging procedure using a sliding window technique. Since CP29 mainly acts as a bridge between LHCII and the core complex and since we do not include any source or drain terms, the dynamics here is limited to the exciton propagation within the complex. In our calculations, we initially excite a single pigment and then monitor the propagation of the exciton wave function toward the other pigments inside the CP29 complex. Each of the 13 Chl pigments was excited individually, and the exciton distributions were captured for each case. To this end, Fig. 10(a) shows the decay of an excitation from individually excited Chl-a pigments. The pigment Chl-a 611 shows the fastest decay since it has the largest excitonic coupling values to its neighbors, whereas for Chl-a 613, the decay is very slow because of its weak interpigment couplings. In Fig. 10(b), we show the case of Chl-a 611 separately including the populations of the other chlorophylls to which the excitation energy is transferred. The population leaves pigment Chl-a 611 exponentially fast and moves to neighboring pigments within a few 100 fs. Since Chl-a 612 is strongly coupled to Chl-a 611, its population gain is very fast within the first 400 fs before the excitation energy is transferred further. At this point, one has to keep in mind that due to the implicit high-temperature approximation in the Ehrenfest approach, the scheme will not lead to a proper thermodynamic equilibrium state but rather to an equal population of all sites. Moreover, it should be mentioned that the population curves become smoother within the increasing number of samples in the averaging procedure, which is limited here due to the finite length of the QM/MM trajectory.

Similar to the Chl-a pigments, the transfer dynamics for the Chl-b molecules is shown in Figs. 10(c) and 10(d). Since the pigments Chl-b 607 and 614 have only weak coupling values to the other chlorophylls, the exciton transfer is expected to be slow from these sites. As one can see in Fig. 10(c), more than 80% of the population is still present on these pigments if they were initially excited. The coupling values of pigment Chl-b 608 are slightly higher, which is also visible in the respective exciton transfer time. However, Chl-b 606 is strongly coupled to its neighboring pigment Chl-a 604 and within about 500 fs, almost the full population is equally shared between these pigments. Moreover, the dynamics continues for a longer time more than 1.5 ps where the population gain of the other pigments is close to zero.

Absorption spectra

The time-averaged system Hamiltonian as shown in Eq. (1) together with the site-dependent spectral densities can be employed to model the linear absorption. While various approximations to calculate the linear absorption $I(\omega)$ are known,[91–93] here we employ one based on Redfield theory,[94,95]

$$I(\omega) \propto \omega\sum_\alpha |\mu_\alpha|^2 D_\alpha(\omega), \tag{13}$$

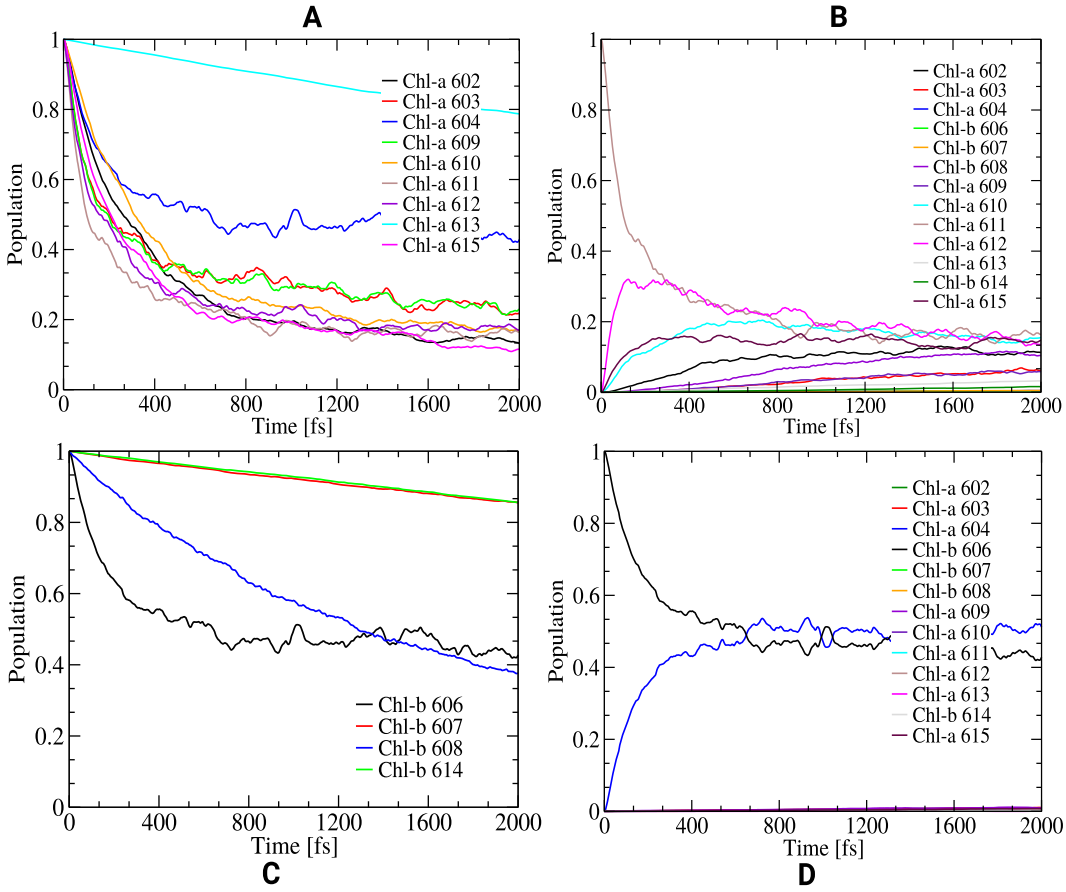

FIG. 10. (a) Decay of the exciton population from different initially excited Chl-a pigments. (b) Population transfer from an initially excited Chl-a 611 pigment to the other pigment molecules inside the CP29 complex. (c) Same as panel (a) but for the Chl-b pigments. (d) Same as panel (b) but for the initially excited Chl-b 606 pigment.

where $\mu_\alpha = \sum_m c_m^\alpha \mu_m$ denotes the excitonic transition dipole moments with μ_m being the transition dipole moments in a site basis. Within a cumulant expansion, the homogeneous line shape $D_\alpha(\omega)$ can be written as

$$D_\alpha(\omega) = \int_{-\infty}^{\infty} e^{-i(\omega_\alpha-\omega)t-g_\alpha(t)-|t|/\tau_\alpha}\, dt, \tag{14}$$

where τ_α and g_α denote the excitonic lifetimes and line shape function for the excitonic state α, respectively. Within Redfield theory, the inverse of the excitonic lifetimes τ_α is given by

$$\tau_\alpha^{-1}(\omega) = \frac{1}{2}\sum_\beta^{\beta\neq\alpha} k_{\alpha\to\beta}. \tag{15}$$

The rate constants can be estimated using the site-dependent spectral densities for $\omega_{\alpha\beta} > 0$ as

$$k_{\alpha\to\beta} = \sum_m |\, c_m^\alpha\,|^2\, |\, c_m^\beta\,|^2 J_m(\omega_{\alpha\beta}) \tag{16}$$

and for $\omega_{\alpha\beta} < 0$ as

$$k_{\beta\to\alpha} = k_{\alpha\to\beta}\, e^{-\hbar\omega_{\alpha\beta}/k_B T}. \tag{17}$$

Moreover, one needs to work out the excitonic line shape functions g_α. When neglecting site energy correlations and fluctuations of the couplings between the site, g_α are connected to their site-dependent counterparts g_m via

$$g_\alpha(t) = \sum_m |\, c_m^\alpha|^4\, g_m(t), \tag{18}$$

where g_m is the site-dependent line shape functions. The latter functions are connected to the site-dependent spectral density J_m through

$$g_m(t) = \int_0^\infty \frac{d\omega}{\hbar\omega^2} J_m(\omega)\Big[(1-\cos(\omega t))\coth\Big(\frac{\hbar\omega}{2k_B T}\Big) + i(\sin(\omega t)-\omega t)\Big]. \tag{19}$$

In the present study, we have calculated the absorption spectra of the CP29 complex at temperatures of 77, 300, and 77 K using the time-averaged Hamiltonian listed in Table I together with the spectral densities for the individual pigments. The transition dipole moments were extracted from the TD-LC-DFTB calculations and averaged over the 1 ns long trajectory. Shown in Fig. 11 is the

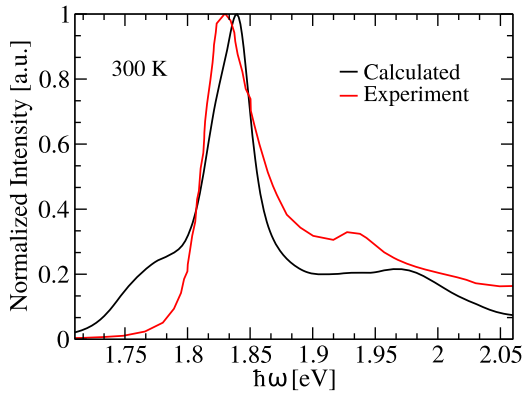

FIG. 11. Absorption spectrum modeled at 300 K compared to an experimental finding at room temperature.[96]

comparison of the calculated and measured absorption spectra[96] at room temperature. The absorption spectrum calculated at low temperature (77 K) is shown in Fig. S8. Because of the overestimation of excitation energy gaps in DFT-based approaches, we have shifted the peak positions of the calculated spectra to match that of the measured ones. The width of the main peak shows a good agreement experiment, although we have not considered any broadening due to static disorder. Moreover, the vibrational sideband toward higher energies shows a nice agreement between theory and experiment. In the calculations, this sideband is due to the high-frequency peaks in the spectral densities. The good agreement of the linear absorption between theory and experiments further validates the present formalism for modeling LH complexes, though the shoulder towards lower frequencies at 300 K and the extra peak at 77 K indicate some possible problems with the DFTB calculations of site energies and/or transition dipole moments. Furthermore, it can be noted that distributions of the excitation energies shown in Figs. S2 and S3 are significantly wider than the main peaks of the absorption spectra. This confirms the earlier finding that the distributions of (excitonic) energy distributions are in general not very good approximations for absorption spectra.[93]

CONCLUSIONS

The molecular details and the mechanism of the pH-induced photoprotective mechanism in higher plants have raised significant interest in recent years.[9–11,34] It has been proposed that under excess sunlight, an enhanced pH gradient is established across the thylakoid membrane embedding the PSII complex, which induces conformational changes in the associated proteins in order to release the extra energy as heat. In this process, the major antenna complex LHCII has been identified as one of the key players. Furthermore, recent studies show that the minor antenna complex CP29 that acts as a bridge between LHCII and the reaction center is also involved in this quenching mechanism.[12,13,19] In order to study the energy transfer dynamics involved in this system, the bath-induced spectral density is one of the key ingredients in tight-binding descriptions of the underlying processes.

Earlier theoretical approaches for calculating spectral densities were based on classical MD simulations for the ground state dynamics followed by excited state calculations. In these calculations, the high frequency regions of these spectral densities were rather inaccurately described since standard classical force fields cannot properly describe the intramolecular vibrational dynamics of the respective pigments. To avoid this issue, a QM/MM MD ground state dynamics has to be performed. Using DFT approaches with a reasonable functional and basis set is numerically quite expensive. To this end, we performed the ground state QM/MM MD dynamics followed by excited state calculations within the numerically efficient DFTB formalism. This procedure yielded spectral densities with a remarkable accuracy compared to experimental findings. In this study, we have extended this multiscale approach to the CP29 minor antenna complex containing Chl-a and Chl-b molecules as primary pigments.

The trend of the site energy ladder is in good agreement with other computed and measured results, while the values of the site energies are overestimated due to the well-known issues of DFT approaches with overestimating excitation energy gaps.[48,57] For this reason, we introduced a common shift for the present site energies toward the experimental energies to match the average experimental results. Moreover, as expected, the average site energies based on TD-LC-DFTB calculations along DFTB-QM/MM MD trajectories for the Chl-b molecules in the CP29 complex are slightly blue shifted compared to those of the Chl-a chromophores. However, in the energy gap autocorrelation functions and spectral densities, such a difference is not visible since both Chl molecules produce very similar correlation functions and spectral densities. Moreover, the accuracy of the present method can also be judged by comparing with spectral densities obtained from experiments. Most of the major peaks are found at the same frequencies and the intensities show a very good agreement with experimental results. In the present findings, the lower frequency peaks are, however, moderately overestimated which needs to be further analyzed.

Moreover, in order to check the robustness and reliability of the present scheme, two different variants of classical force fields, i.e., AMBER and OPLS, were employed together with the DFTB approach in a QM/MM fashion. The description of the environment with the two different force fields resulted in almost indistinguishable spectral densities, which supports the fact that either of the two force fields might be used when modeling LH complexes within a QM/MM framework. Moreover, based on our previous study on the FMO complex of green sulfur bacteria, the range of the site energy fluctuations of BChl pigments is noticeably smaller than that of the Chl molecule calculated in the present study and in a previous one for the LHCII complex.[57] This fact is also reflected in the amplitudes of the spectral density peaks, which are lower for the FMO complex when compared to those of the two plant systems. In experimental measurements, the spectral density of the FMO complex shows more peaks since it contains one C=C double bond less in the Mg-porphyrin rings compared to the bacterial systems. However, in our theoretical calculations, we found a smaller number of peaks since some of them seem to be merged to form peaks.

In addition to determining site energies and spectral densities, we have also calculated the excitonic couplings based on the TrESP approach and constructed a time-averaged system Hamiltonian. Since the QM/MM MD simulation is still numerically expensive

when taking several pigments into account simultaneously, the couplings were determined from a 200 ns classical MD trajectory and combined with the site energies from the 1 ns QM/MM MD trajectory. This mixed approach is reasonable as the coupling fluctuations are less significant during the energy transfer dynamics.[48,79] A time-averaged version of the Hamiltonian together with the obtained spectral densities can possibly be employed in future density matrix-based studies. In the present study, however, the time-averaged coupling values together with the time-dependent site energies from the first set of 60 ps QM/MM MD trajectories have been used in an ensemble-averaged wave packet scheme. Using such an approach, one can analyze how excitons are transferred between the individual pigments and how they spread within the system.

Moreover, we have calculated the absorption spectrum within a standard approach using the time-averaged Hamiltonian and the site-dependent spectral densities as key inputs. The calculated spectrum shows a nice agreement with the experimental counterpart. Interestingly, the high-energy peaks in the spectral density lead to a shoulder in the absorption spectrum, which is also found in experiment. This finding further validates the robustness and reliability of our present multiscale method, which can be applied to various LH complexes of plants, bacteria, and algae.

In summary, we have established a multiscale protocol with the numerically efficient DFTB method, which can accurately describe spectral densities that are key quantities for modeling of photochemical processes.[48,57] In the present study, the approach has been tested once more for an important plant LH system and it has been shown that the scheme produces reproducible, robust, and reliable results based on different simulations and various LH complexes. To this end, the multiscale protocol was utilized for the CP29 complex, which recently has gained quite some interest because of its active participation in the non-photochemical quenching.[22,83] The outcome of the present calculations is the site energy, couplings, and most importantly the spectral densities. Moreover, we have also presented a realistic time-averaged Hamiltonian and obtained results for the exciton dynamics based on a time-dependent Hamiltonian. In conclusion, the present study has shed light on the electronic properties of the pigment molecules in the CP29 complex as well as on the exciton–phonon and exciton–vibrational couplings within this pigment–protein aggregate. This molecular-level insight can be used in future investigations of this biologically relevant complex or of the whole PSII machinery. Simulations of entire bacterial photosynthetic organelles became possible recently,[97] while similar simulations of larger aggregates of plant pigment–protein complexes are yet to come.

SUPPLEMENTARY MATERIAL

See the supplementary material for additional figures and descriptions on site energy distributions, spectral densities, and the absorption spectrum at low temperature.

ACKNOWLEDGMENTS

The authors acknowledge the support by the DFG through Grant No. KL-1299/18-1 as well as through the Research Training Group 2247 "Quantum Mechanical Materials Modeling."

DATA AVAILABILITY

The data that support the findings of this study are available from the corresponding author upon reasonable request.

REFERENCES

[1] R. E. Blankenship, *Molecular Mechanisms of Photosynthesis*, 2nd ed. (Wiley, 2014).
[2] G. S. Engel, T. R. Calhoun, E. L. Read, T.-K. Ahn, T. Mančal, Y.-C. Cheng, R. E. Blankenship, and G. R. Fleming, "Evidence for wavelike energy transfer through quantum coherence in photosynthetic systems," Nature **446**, 782–786 (2007).
[3] E. Collini and G. D. Scholes, "Coherent intrachain energy migration in a conjugated polymer at room temperature," Science **323**, 369–373 (2009).
[4] E. Collini, C. Y. Wong, K. E. Wilk, P. M. G. Curmi, P. Brumer, and G. D. Scholes, "Coherently wired light-harvesting in photosynthetic marine algae at ambient temperature," Nature **463**, 644–647 (2010).
[5] G. Panitchayangkoon, D. Hayes, K. A. Fransted, J. R. Caram, E. Harel, J. Wen, R. E. Blankenship, and G. S. Engel, "Long-lived quantum coherence in photosynthetic complexes at physiological temperature," Proc. Natl. Acad. Sci. U. S. A. **107**, 12766–12770 (2010).
[6] J. Cao *et al.*, "Quantum biology revisited," Sci. Adv. **6**, eaaz4888 (2020).
[7] H.-G. Duan, V. I. Prokhorenko, R. J. Cogdell, K. Ashraf, A. L. Stevens, M. Thorwart, and R. J. D. Miller, "Nature does not rely on long-lived electronic quantum coherence for photosynthetic energy transfer," Proc. Natl. Acad. Sci. U. S. A. **114**, 8493 (2017).
[8] E. Thyrhaug, R. Tempelaar, M. J. P. Alcocer, K. Žídek, D. Bína, J. Knoester, T. L. C. Jansen, and D. Zigmantas, "Identification and characterization of diverse coherences in the Fenna-Matthews-Olson complex," Nat. Chem. **10**, 780–786 (2018).
[9] A. V. Ruban, R. Berera, C. Ilioaia, I. H. M. Van Stokkum, J. T. M. Kennis, A. A. Pascal, H. Van Amerongen, B. Robert, P. Horton, and R. Van Grondelle, "Identification of a mechanism of photoprotective energy dissipation in higher plants," Nature **450**, 575 (2007).
[10] A. V. Ruban, M. P. Johnson, and C. D. P. Duffy, "The photoprotective molecular switch in the photosystem II antenna," Biochim. Biophys. Acta, Bioenerg. **1817**, 167–181 (2012).
[11] J. Chmeliov, A. Gelzinis, E. Songaila, R. Augulis, C. D. P. Duffy, A. V. Ruban, and L. Valkunas, "The nature of self-regulation in photosynthetic light-harvesting antenna," Nat. Plants **2**, 16045 (2016).
[12] L. Tian, W. J. Nawrocki, X. Liu, I. Polukhina, I. H. M. Van Stokkum, and R. Croce, "pH dependence, kinetics and light-harvesting regulation of nonphotochemical quenching in *Chlamydomonas*," Proc. Natl. Acad. Sci. U. S. A. **116**, 8320–8325 (2019).
[13] L. Nicol, W. J. Nawrocki, and R. Croce, "Disentangling the sites of non-photochemical quenching in vascular plants," Nat. Plants **5**, 1177–1183 (2019).
[14] J. M. Buck, J. Sherman, C. R. Bártulos, M. Serif, M. Halder, J. Henkel, A. Falciatore, J. Lavaud, M. Y. Gorbunov, P. G. Kroth *et al.*, "Lhcx proteins provide photoprotection via thermal dissipation of absorbed light in the diatom *Phaeodactylum tricornutum*," Nat. Commun. **10**, 4167 (2019).
[15] G. de la Cruz Valbuena, F. V. A. Camargo, R. Borrego-Varillas, F. Perozeni, C. D'Andrea, M. Ballottari, and G. Cerullo, "Molecular mechanisms of nonphotochemical quenching in the LHCSR3 protein of *Chlamydomonas reinhardtii*," J. Phys. Chem. Lett. **10**, 2500–2505 (2019).
[16] X.-P. Li, O. Björkman, C. Shih, A. R. Grossman, M. Rosenquist, S. Jansson, and K. K. Niyogi, "A pigment-binding protein essential for regulation of photosynthetic light harvesting," Nature **403**, 391 (2000).
[17] V. Correa-Galvis, G. Poschmann, M. Melzer, K. Stühler, and P. Jahns, "PsbS interactions involved in the activation of energy dissipation in *Arabidopsis*," Nat. Plants **2**, 15225 (2016).
[18] N. Liguori, S. R. R. Campos, A. M. Baptista, and R. Croce, "Molecular anatomy of plant photoprotective switches: The sensitivity of PsbS to the environment, residue by residue," J. Phys. Chem. Lett. **10**, 1737–1742 (2019).
[19] Z. Guardini, M. Bressan, R. Caferri, R. Bassi, and L. Dall'Osto, "Identification of a pigment cluster catalysing fast photoprotective quenching response in CP29," Nat. Plants **6**, 303–313 (2020).

[20]A. V. Ruban, "Light harvesting control in plants," FEBS Lett. **592**, 3030–3039 (2018).
[21]L. Dall'Osto, S. Cazzaniga, M. Bressan, D. Paleček, K. Židek, K. K. Niyogi, G. R. Fleming, D. Zigmantas, and R. Bassi, "Two mechanisms for dissipation of excess light in monomeric and trimeric light-harvesting complexes," Nat. Plants **3**, 17033 (2017).
[22]M. Son and G. S. Schlau-Cohen, "Flipping a protein switch: Carotenoid-mediated quenching in plants," Chem **5**, 2749–2750 (2019).
[23]Z. Liu, H. Yan, K. Wang, T. Kuang, J. Zhang, L. Gui, X. An, and W. Chang, "Crystal structure of spinach major light-harvesting complex at 2.72 Å resolution," Nature **428**, 287–292 (2004).
[24]F. Müh, M. E.-A. Madjet, and T. Renger, "Structure-based identification of energy sinks in plant light-harvesting complex II," J. Phys. Chem. B **114**, 13517–13535 (2010).
[25]F. Müh and T. Renger, "Refined structure-based simulation of plant light-harvesting complex II: Linear optical spectra of trimers and aggregates," Biochim. Biophys. Acta, Bioenerg. **1817**, 1446–1460 (2012).
[26]C. D. P. Duffy, J. Chmeliov, M. Macernis, J. Sulskus, L. Valkunas, and A. V. Ruban, "Modeling of fluorescence quenching by lutein in the plant light-harvesting complex LHCII," J. Phys. Chem. B **117**, 10974–10986 (2013).
[27]J. Chmeliov, W. P. Bricker, C. Lo, E. Jouin, L. Valkunas, A. V. Ruban, and C. D. P. Duffy, "An 'all pigment' model of excitation quenching in LHCII," Phys. Chem. Chem. Phys. **17**, 15857–15867 (2015).
[28]X. Pan, M. Li, T. Wan, L. Wang, C. Jia, Z. Hou, X. Zhao, J. Zhang, and W. Chang, "Structural insights into energy regulation of light-harvesting complex CP29 from spinach," Nat. Struct. Mol. Biol. **18**, 309–315 (2011).
[29]X. Wei, X. Su, P. Cao, X. Liu, W. Chang, M. Li, X. Zhang, and Z. Liu, "Structure of spinach photosystem II-LHCII supercomplex at 3.2 Å resolution," Nature **534**, 69–74 (2016).
[30]F. Müh, D. Lindorfer, M. Schmidt am Busch, and T. Renger, "Towards a structure-based exciton Hamiltonian for the CP29 antenna of photosystem II," Phys. Chem. Chem. Phys. **16**, 11848–11863 (2014).
[31]S. Jurinovich, L. Viani, I. G. Prandi, T. Renger, and B. Mennucci, "Towards an *ab initio* description of the optical spectra of light-harvesting antennae: Application to the CP29 complex of photosystem II," Phys. Chem. Chem. Phys. **17**, 14405–14416 (2015).
[32]K. F. Fox, C. Ünlü, V. Balevičius, Jr., B. N. Ramdour, C. Kern, X. Pan, M. Li, H. van Amerongen, and C. D. P. Duffy, "A possible molecular basis for photoprotection in the minor antenna proteins of plants," Biochim. Biophys. Acta, Bioenerg. **1859**, 471–481 (2018).
[33]M. Lapillo, E. Cignoni, L. Cupellini, and B. Mennucci, "The energy transfer model of nonphotochemical quenching: Lessons from the minor CP29 antenna complex of plants," Biochim. Biophys. Acta, Bioenerg. **1861**, 148282 (2020).
[34]V. Daskalakis, S. Maity, C. L. Hart, T. Stergiannakos, C. D. P. Duffy, and U. Kleinekathöfer, "Structural basis for allosteric regulation in the major antenna trimer of photosystem II," J. Phys. Chem. B **123**, 9609–9615 (2019).
[35]V. Daskalakis, S. Papadatos, and U. Kleinekathöfer, "Fine tuning of the photosystem II major antenna mobility within the thylakoid membrane of higher plants," Biochim. Biophys. Acta, Rev. Biomembr. **1861**, 183059 (2019).
[36]S. Maity, A. Gelessus, V. Daskalakis, and U. Kleinekathöfer, "On a chlorophyll-caroteinoid coupling in LHCII," Chem. Phys. **526**, 110439 (2019).
[37]V. Daskalakis, "Protein-protein interactions within photosystem II under photoprotection: The synergy between CP29 minor antenna, subunit S (PsbS) and zeaxanthin at all-atom resolution," Phys. Chem. Chem. Phys. **20**, 11843–11855 (2018).
[38]V. Daskalakis, S. Papadatos, and T. Stergiannakos, "The conformational phase space of the photoprotective switch in the major light harvesting complex II," Chem. Commun. **56**, 11215–11218 (2020).
[39]C. Kreisbeck, T. Kramer, and A. Aspuru-Guzik, "Scalable high-performance algorithm for the simulation of exciton dynamics. Application to the light-harvesting complex II in the presence of resonant vibrational modes," J. Chem. Theory Comput. **10**, 4045–4054 (2014).
[40]J. J. J. Roden, D. I. G. Bennett, and K. B. Whaley, "Long-range energy transport in photosystem II," J. Chem. Phys. **144**, 245101 (2016).
[41]V. May and O. Kühn, *Charge and Energy Transfer in Molecular Systems*, 3rd ed. (Wiley–VCH, 2011).
[42]A. Damjanović, I. Kosztin, U. Kleinekathöfer, and K. Schulten, "Excitons in a photosynthetic light-harvesting system: A combined molecular dynamics, quantum chemistry and polaron model study," Phys. Rev. E **65**, 031919 (2002).
[43]C. Olbrich and U. Kleinekathöfer, "Time-dependent atomistic view on the electronic relaxation in light-harvesting system II," J. Phys. Chem. B **114**, 12427–12437 (2010).
[44]C. Olbrich, J. Strümpfer, K. Schulten, and U. Kleinekathöfer, "Theory and simulation of the environmental effects on FMO electronic transitions," J. Phys. Chem. Lett. **2**, 1771–1776 (2011).
[45]S. Shim, P. Rebentrost, S. Valleau, and A. Aspuru-Guzik, "Atomistic study of the long-lived quantum coherences in the Fenna-Matthew-Olson complex," Biophys. J. **102**, 649–660 (2012).
[46]M. Aghtar, J. Strümpfer, C. Olbrich, K. Schulten, and U. Kleinekathöfer, "Different types of vibrations interacting with electronic excitations in phycoerythrin 545 and Fenna-Matthews-Olson antenna systems," J. Phys. Chem. Lett. **5**, 3131–3137 (2014).
[47]M. K. Lee and D. F. Coker, "Modeling electronic-nuclear interactions for excitation energy transfer processes in light-harvesting complexes," J. Phys. Chem. Lett. **7**, 3171–3178 (2016).
[48]S. Maity, B. M. Bold, J. D. Prajapati, M. Sokolov, T. Kubař, M. Elstner, and U. Kleinekathöfer, "DFTB/MM molecular dynamics simulations of the FMO light-harvesting complex," J. Phys. Chem. Lett. **11**, 8660–8667 (2020).
[49]C. Curutchet and B. Mennucci, "Quantum chemical studies of light harvesting," Chem. Rev. **117**, 294–343 (2017).
[50]M. K. Lee, P. Huo, and D. F. Coker, "Semiclassical path integral dynamics: Photosynthetic energy transfer with realistic environment interactions," Annu. Rev. Phys. Chem. **67**, 639–668 (2016).
[51]C. W. Kim and Y. M. Rhee, "Constructing an interpolated potential energy surface of a large molecule: A case study with bacteriochlorophyll a model in the Fenna-Matthews-Olson complex," J. Chem. Theory Comput. **12**, 5235–5246 (2016).
[52]C. W. Kim, B. Choi, and Y. M. Rhee, "Excited state energy fluctuations in the Fenna-Matthews-Olson complex from molecular dynamics simulations with interpolated chromophore potentials," Phys. Chem. Chem. Phys. **20**, 3310 (2018).
[53]D. Padula, M. H. Lee, K. Claridge, and A. Troisi, "Chromophore-dependent intramolecular exciton-vibrational coupling in the FMO complex: Quantification and importance for exciton dynamics," J. Phys. Chem. B **121**, 10026–10035 (2017).
[54]A. M. Rosnik and C. Curutchet, "Theoretical characterization of the spectral density of the water-soluble chlorophyll-binding protein from combined quantum mechanics/molecular mechanics molecular dynamics simulations," J. Chem. Theory Comput. **11**, 5826–5837 (2015).
[55]S. M. Blau, D. I. G. Bennett, C. Kreisbeck, G. D. Scholes, and A. Aspuru-Guzik, "Local protein solvation drives direct down-conversion in phycobiliprotein PC645 via incoherent vibronic transport," Proc. Natl. Acad. Sci. U. S. A. **115**, E3342–E3350 (2018).
[56]M. Elstner, D. Porezag, G. Jungnickel, J. Elsner, M. Haugk, T. Frauenheim, S. Suhai, and G. Seifert, "Self-consistent-charge density-functional tight-binding method for simulations of complex materials properties," Phys. Rev. B **58**, 7260–7268 (1998).
[57]S. Maity, V. Daskalakis, M. Elstner, and U. Kleinekathöfer, "Multiscale QM/MM molecular dynamics simulations of the trimeric major light-harvesting complex II," Phys. Chem. Chem. Phys. **23**, 7407–7417 (2021).
[58]Y. Duan, C. Wu, S. Chowdhury, M. C. Lee, G. Xiong, W. Zhang, R. Yang, P. Cieplak, R. Luo, T. Lee *et al.*, "A point-charge force field for molecular mechanics simulations of proteins based on condensed-phase quantum mechanical calculations," J. Comput. Chem. **24**, 1999–2012 (2003).
[59]M. J. Abraham, T. Murtola, R. Schulz, S. Páll, J. C. Smith, B. Hess, and E. Lindahl, "GROMACS: High performance molecular simulations through multi-level parallelism from laptops to supercomputers," SoftwareX **1-2**, 19–25 (2015).
[60]M. Ceccarelli, P. Procacci, and M. Marchi, "An *ab initio* force field for the cofactors of bacterial photosynthesis," J. Comput. Chem. **24**, 129–132 (2003).

[61] L. Zhang, D.-A. Silva, Y. Yan, and X. Huang, "Force field development for cofactors in the photosystem II," J. Comput. Chem. **33**, 1969–1980 (2012).
[62] I. G. Prandi, L. Viani, O. Andreussi, and B. Mennucci, "Combining classical molecular dynamics and quantum mechanical methods for the description of electronic excitations: The case of carotenoids," J. Comput. Chem. **37**, 981–991 (2016).
[63] S. Jo, T. Kim, V. G. Iyer, and W. Im, "CHARMM-GUI: A web-based graphical user interface for CHARMM," J. Comput. Chem. **29**, 1859–1865 (2008).
[64] A. W. S. Da Silva and W. F. Vranken, "ACPYPE-antechamber Python parser interface," BMC Res. Notes **5**, 367 (2012).
[65] M. E. Madjet, A. Abdurahman, and T. Renger, "Intermolecular Coulomb couplings from *ab initio* electrostatic potentials: Application to optical transitions of strongly coupled pigments in photosynthetic antennae and reaction centers," J. Phys. Chem. B **110**, 17268–17281 (2006).
[66] C. Olbrich, T. L. C. Jansen, J. Liebers, M. Aghtar, J. Strümpfer, K. Schulten, J. Knoester, and U. Kleinekathoöfer, "From atomistic modeling to excitation dynamics and two-dimensional spectra of the FMO light-harvesting complex," J. Phys. Chem. B **115**, 8609–8621 (2011).
[67] X. Su, J. Ma, X. Wei, P. Cao, D. Zhu, W. Chang, Z. Liu, X. Zhang, and M. Li, "Structure and assembly mechanism of plant $C_2S_2M_2$-type PSII-LHCII supercomplex," Science **357**, 815–820 (2017).
[68] B. M. Bold, M. Sokolov, S. Maity, M. Wanko, P. M. Dohmen, J. J. Kranz, U. Kleinekathöfer, S. Höfener, and M. Elstner, "Benchmark and performance of long-range corrected time-dependent density functional tight binding (LC-TD-DFTB) on rhodopsins and light-harvesting complexes," Phys. Chem. Chem. Phys. **22**, 10500–10518 (2020).
[69] M. Gaus, Q. Cui, and M. Elstner, "DFTB3: Extension of the self-consistent-charge density-functional tight-binding method (SCC-DFTB)," J. Chem. Theory Comput. **7**, 931–948 (2011).
[70] M. Gaus, A. Goez, and M. Elstner, "Parametrization and benchmark of DFTB3 for organic molecules," J. Chem. Theory Comput. **9**, 338–354 (2013).
[71] T. Kubař, K. Welke, and G. Groenhof, "New QM/MM implementation of the DFTB3 method in the Gromacs package," J. Comput. Chem. **36**, 1978–1989 (2015).
[72] B. Hourahine *et al.*, "DFTB+, a software package for efficient approximate density functional theory based atomistic simulations," J. Chem. Phys. **152**, 124101 (2020).
[73] J. J. Kranz, M. Elstner, B. Aradi, T. Frauenheim, V. Lutsker, A. D. Garcia, and T. A. Niehaus, "Time-dependent extension of the long-range corrected density functional based tight-binding method," J. Chem. Theory Comput. **13**, 1737–1747 (2017).
[74] T. Lu and F. Chen, "Multiwfn: A multifunctional wavefunction analyzer," J. Comput. Chem. **33**, 580–592 (2012).
[75] F. Neese, "Software update: The ORCA program system, version 4.0," Wiley Interdiscip. Rev.: Comput. Mol. Sci. **8**, e1327 (2018).
[76] R. S. Knox and B. Q. Spring, "Dipole strengths in the chlorophylls," Photochem. Photobiol. **77**, 497–501 (2003).
[77] M. Aghtar, J. Liebers, J. Strümpfer, K. Schulten, and U. Kleinekathöfer, "Juxtaposing density matrix and classical path-based wave packet dynamics," J. Chem. Phys. **136**, 214101 (2012).
[78] T. L. C. Jansen, "Simple quantum dynamics with thermalization," J. Phys. Chem. A **122**, 172–183 (2018).
[79] M. Aghtar, U. Kleinekathöfer, C. Curutchet, and B. Mennucci, "Impact of electronic fluctuations and their description on the exciton dynamics in the light-harvesting complex PE545," J. Phys. Chem. B **121**, 1330–1339 (2017).
[80] S. Valleau, A. Eisfeld, and A. Aspuru-Guzik, "On the alternatives for bath correlators and spectral densities from mixed quantum-classical simulations," J. Chem. Phys. **137**, 224103 (2012).
[81] C. Curutchet, G. D. Scholes, B. Mennucci, and R. Cammi, "How solvent controls electronic energy transfer and light harvesting: Toward a quantum-mechanical description of reaction field and screening effects," J. Phys. Chem. B **111**, 13253–13265 (2007).
[82] M. Jassas, J. Chen, A. Khmelnitskiy, A. P. Casazza, S. Santabarbara, and R. Jankowiak, "Structure-based exciton Hamiltonian and dynamics for the reconstituted wild-type CP29 protein antenna complex of the photosystem II," J. Phys. Chem. B **122**, 4611–4624 (2018).
[83] V. Mascoli, V. Novoderezhkin, N. Liguori, P. Xu, and R. Croce, "Design principles of solar light harvesting in plants: Functional architecture of the monomeric antenna CP29," Biochim. Biophys. Acta, Rev. Bioenerg. **1861**, 148156 (2020).
[84] D. I. G. Bennett, K. Amarnath, and G. R. Fleming, "A structure-based model of energy transfer reveals the principles of light harvesting in photosystem II supercomplexes," J. Am. Chem. Soc. **135**, 9164–9173 (2013).
[85] V. I. Novoderezhkin, M. A. Palacios, H. van Amerongen, and R. van Grondelle, "Energy-transfer dynamics in the LHCII complex of higher plants: Modified Redfield approach," J. Phys. Chem. B **108**, 10363 (2004).
[86] A. Kell, X. Feng, M. Reppert, and R. Jankowiak, "On the shape of the phonon spectral density in photosynthetic complexes," J. Phys. Chem. B **117**, 7317–7323 (2013).
[87] S. Chandrasekaran, M. Aghtar, S. Valleau, A. Aspuru-Guzik, and U. Kleinekathöfer, "Influence of force fields and quantum chemistry approach on spectral densities of BChl *a* in solution and in FMO proteins," J. Phys. Chem. B **119**, 9995–10004 (2015).
[88] W. L. Jorgensen and J. Tirado-Rives, "The OPLS [optimized potentials for liquid simulations] potential functions for proteins, energy minimizations for crystals of cyclic peptides and crambin," J. Am. Chem. Soc. **110**, 1657–1666 (1988).
[89] M. Rätsep and A. Freiberg, "Electron-phonon and vibronic couplings in the FMO bacteriochlorophyll *a* antenna complex studied by difference fluorescence line narrowing," J. Lumin. **127**, 251–259 (2007).
[90] H. Rahman and U. Kleinekathöfer, "Chebyshev hierarchical equations of motion for systems with arbitrary spectral densities and temperatures," J. Chem. Phys. **150**, 244104 (2019).
[91] M. Schröder, U. Kleinekathöfer, and M. Schreiber, "Calculation of absorption spectra for light-harvesting systems using non-Markovian approaches as well as modified Redfield theory," J. Chem. Phys. **124**, 084903 (2006).
[92] T.-C. Dinh and T. Renger, "Towards an exact theory of linear absorbance and circular dichroism of pigment-protein complexes: Importance of non-secular contributions," J. Chem. Phys. **142**, 034104 (2015).
[93] T. J. Zuehlsdorff, A. Montoya-Castillo, J. A. Napoli, T. E. Markland, and C. M. Isborn, "Optical spectra in the condensed phase: Capturing anharmonic and vibronic features using dynamic and static approaches," J. Chem. Phys. **151**, 074111 (2019).
[94] V. I. Novoderezhkin and R. van Grondelle, "Physical origins and models of energy transfer in photosynthetic light-harvesting," Phys. Chem. Chem. Phys. **12**, 7352–7365 (2010).
[95] T. Renger and F. Müh, "Understanding photosynthetic light-harvesting: A bottom up theoretical approach," Phys. Chem. Chem. Phys. **15**, 3348–3371 (2013).
[96] E. Belgio, G. Tumino, S. Santabarbara, G. Zucchelli, and R. Jennings, "Reconstituted CP29: Multicomponent fluorescence decay from an optically homogeneous sample," Photosynth. Res. **111**, 53–62 (2012).
[97] A. Singharoy *et al.*, "Atoms to phenotypes: Molecular design principles of cellular energy metabolism," Cell **179**, 1098–1111.e23 (2019).